DOI: 10.1002/cjoc.201201151

Synthesis of Bi-doped TiO_2 Nanotubes and Enhanced Photocatalytic Activity for Hydrogen Evolution from Glycerol Solution

Wenxi Zhao,[b] Xitao Wang,*,[a] Huanxin Sang,[b] and Kang Wang[a]

[a] *Tianjin Key Laboratory of Applied Catalysis Science and Technology, College of Chemical Engineering and Technology, Tianjin University, Tianjin 300072, China*
[b] *Tianjin Academy of Environmental Sciences, Tianjin 300191, China*

Bi-doped TiO_2 nanotubes with variable Bi/Ti ratios were synthesized by hydrothermal treatment in 10 mol•L^{-1} NaOH (aq.) through using Bi-doped TiO_2 particles derived from conventional sol-gel method as starting materials. The effects of Bi content on the morphology, textural properties, photo absorption and photocatalytic activity of TiO_2 nanotubes were investigated. The scanning electron microscopy (SEM), transmission electron microscopy (TEM), X-ray diffraction (XRD) and X-ray photoelectron spectroscopy (XPS) observations of the obtained samples revealed the formation of titanate nanotube structure doped with Bi, which exists as a higher oxidation state than Bi^{3+}. Bi-doping TiO_2 nanotubes exhibited an extension of light absorption into the visible region and improved photocatalytic activities for hydrogen production from a glycerol/water mixed solution as compared with pure TiO_2 nanotubes. There was an optimal Bi-doped content for the photocatalytic hydrogen production, and high content of Bi would retard the phase transition of titanate to anatase and result in morphology change from nanotube to nanobelt, which in turn decreases the photocatlytic activity for hydrogen evolution.

Keywords Bi-doped, TiO_2 nanotubes, photocatalytic hydrogen evolution, glycerol solution

Introduction

In the last two decades, a number of efforts have been made to explore the photocatalysts used for water splitting to generate hydrogen by absorbing solar energy.[1-3] TiO_2 is the most investigated photocatalytic material due to its particular properties.[4-6] Nevertheless, the ability of water splitting of TiO_2 is limited due to its wide band gap and narrow spectra range for light response. In order to make better use of solar energy, many attempts have been proposed to sensitize TiO_2 in the visible-light region.[7-9] Recently, the fabrication of TiO_2 nanotubes has attracted enormous attention owing to its highly ordered tube structure, high surface-to-volume ratio and large specific surface area. Besides that, they would enhance the light absorption, and benefit the efficiency for electron transportation.

Bi_2O_3 is a significant metal-oxide semiconductor with a direct band gap of 2.8 eV, which can be excited by visible light, but the photocatalytic activity of Bi_2O_3 is low due to the photocorrosion and fast recombination of photogenerated electron-hole pairs.[10] In recent years, the development of Bi_2O_3-TiO_2 composite photocatalyst that can work effectively under visible light irradiation with photochemical stability is a very hot topic in photocatalytic research.[11-16] Zhang *et al.* report the controllable and reproducible synthesis of a Bi-doped ordered mesoporous TiO_2.[15] They found that Bi species exist in various forms in the doped samples, and that the suitable doping of Bi significantly enhanced photocatalytic oxidation of phenol and reduction of chromium in aqueous suspension. Ji *et al.* prepared the Bi-doped anatase TiO_2 nanobelts from layer-structural titanate nanobelts using two-step hydrothermal treatment approach.[16] The ultraviolet-visible (UV-vis) absorption spectra show that the absorption edge for the samples with Bi^{3+} has red shift as compared with that of undoped TiO_2 nanobelts, and correspondingly, the photocatalytic degradation of methylene blue under visible-light illumination is enhanced with the increase of Bi-doping content.

Although a lot of researches have reported the Bi-doped TiO_2 with highly photocatalytic activities under the visible-light irradiation, there is no work focusing on the preparation and photocatalytic activity of Bi-doped TiO_2 nanotubes for hydrogen production. Therefore, in the present work, we systematically studied the effects of Bi-doping amount on the morphology, photo absorption and photocatalytic hydrogen production from a glycerol/water mixed solution under UV and solar-sim-

* E-mail: wangxt@tju.edu.cn
Received November 20, 2012; accepted January 13, 2013; published online March 1, 2013.

ulated light irradiation over nanotube in a fixed bed flow-type reactor.

Experimental

Preparation of photocatalysts

Bi-doped TiO_2 nanoparticles with different Bi/Ti molar ratios were prepared by sol-gel method as described in our previous work.[17] Bi-doped TiO_2 nanotubes were prepared by hydrothermal method. In a typical synthesis, 0.5 g of the as-prepared Bi-TiO_2 nanoparticle was dispersed in 10 mol•L^{-1} NaOH (aq.) and then was transferred into a 100 mL Teflon-lined autoclave. The autoclave was held at 403 K for 48 h. After cooling down to the room temperature, the sample was washed by deionized water, and then treated by 0.5 mol•L^{-1} HCl (aq.) for 12 h. The suspension was filtered and washed with deionized water again and dried at 393 K. According to the Bi content of starting materials, the Bi-doped TiO_2 nanotubes were named *x*-BT NTs (*x*%= Bi/Ti molar ratio).

Characterization of photocatalysts

The concentration of Bi was measured by ICP-AES (Varian, VISTA-MPX). The measurement of the specific surface area (S_{BET}) was carried out at 77 K on Quantachrome SI instrument by using the nitrogen adsorption/desorption method. Morphologies of the prepared samples were observed with a Nova Nano430 scanning electron microscopy (SEM) and JEOL 2010F transmission electron microscopy (TEM). X-ray diffraction (XRD) data of the samples were recorded on a D/MAX-2500 automatic powder diffractometer equipped with the Cu Kα radiation (λ=0.15418 nm). Raman spectra were obtained using an FT-Raman spectrometer (Bruke, RFS 100/S). X-ray photoelectron spectroscopy (XPS) measurements were measured on a Thermo SCIENTIFIC ESCALAB 250 with a resolution of 0.3—1.0 eV, using nonmonochromatized Al Kα X-ray as the excitation source. Binding energy was calibrated with respected to the signal for C 1s of 284.8 eV. UV-visible diffusive reflectance spectra (UV-Vis DRS) were recorded on a Perkin Elmer-Lambda 35 UV-Vis spectrometer.

Photoactivity measurement

Photocatalysis tests were carried out under UV and solar-simulated light irradiation. The reaction apparatus were the same with the reference.[18] Two similar apparatuses were used for the photocalytic activity test, each consisting of light source, cooling system, inner irradiation-type quartz photoreactor and online analysis system. Two different light sources were used in the present study: (a) a UV light source (high-pressure Hg lamp, 125 W), (b) a solar simulated light source (Xe lamp, 500 W). The temperature of the irradiated surface of the catalyst was monitored by a thermocouple directly inserted into the catalyst bed. In a typical reaction, an 80 mg catalyst mixed with 5 mL quartz sand was loaded into the reactor and afterwards 10 mL 5% glycerol solution was added to the reactor dropwise. Argon gas flow of 20 mL/min was made to pass through the reactor to collect and transfer gaseous products to the online gas chromatography equipped with a thermal conductivity detector.

Results and Discussion

Characterization of photocatalysts

The Bi/Ti molar ratios determined by ICP-AES and XPS and the BET surface area of Bi-TiO_2 nanotubes are summarized in Table 1. It can be seen that the element of Bi is detected in Bi-doped samples, which shows that Bi element has been successfully doped into the TiO_2 structure. For three Bi-doped samples, the Bi/Ti molar ratios obtained by ICP-AES and XPS are very close, showing that the Bi element is uniformly distributed in TiO_2 structure. However, the content of Bi determined by ICP and XPS is obviously lower than the calculated data, indicating the loss of Bi element. This can result from the dissolving in the hydrothermal alkali treatment or acid-washing during the preparation of nanotubes. The specific surface areas of TiO_2 and Bi-TiO_2 nanotubes are in the range of 270—290 m^2/g, which is much higher than both Degussa P_{25} and Bi-doped TiO_2 nanopaticles prepared by the conventional sol-gel method.[19] The specific surface areas of samples are almost not changed when Bi doping amount is lower than 1.0% (A slight drop of surface areas over 0.4-BT NTs and 0.7-BT NTs sample may be due to the experiment errors), and then increase obviously with the further increase in Bi content. The increase of surface areas for 2.0-BT NTs and 5.0-BT NTs samples can be due to the formation of nanobelt structure.

Table 1 Bi/Ti molar ratios, BET surface areas of Bi-TiO_2 nanotubes

Sample	Bi/Ti molar ratio *x*/%			S_{BET}/(m^2•g^{-1})
	Caculated	Obtained		
		ICP	XPS	
TiO_2 NTs	0	0	0	275.7
0.4-BT NTs	0.4	0.28	—	271.1
0.7-BT NTs	0.7	0.45	—	273.3
1.0-BT NTs	1.0	0.76	0.80	277.6
2.0-BT NTs	2.0	1.18	1.30	286.4
5.0-BT NTs	5.0	2.16	2.42	288.2

The SEM and TEM images of Bi-doped TiO_2 nanotubes are shown in Figure 1. The tubular structure is multi-wall nanotube with an inter-shell spacing of around 1—1.5 nm. It can be seen from TEM and HRTEM images that no particle was observed on the wall of nanotubes, indicating the Bi cations may have been doped into the crystal structure of TiO_2. Figure 1

(A)—(E) also showed that the nanobelt structure began to appear and have gradually increased with the increase of Bi doping amount. The 5-BT NTs sample exists almost in the form of complete nanobelt structure. These results show that the excessive amount of Bi will restrain a sheet folding or wrapping to a nanotube structure.

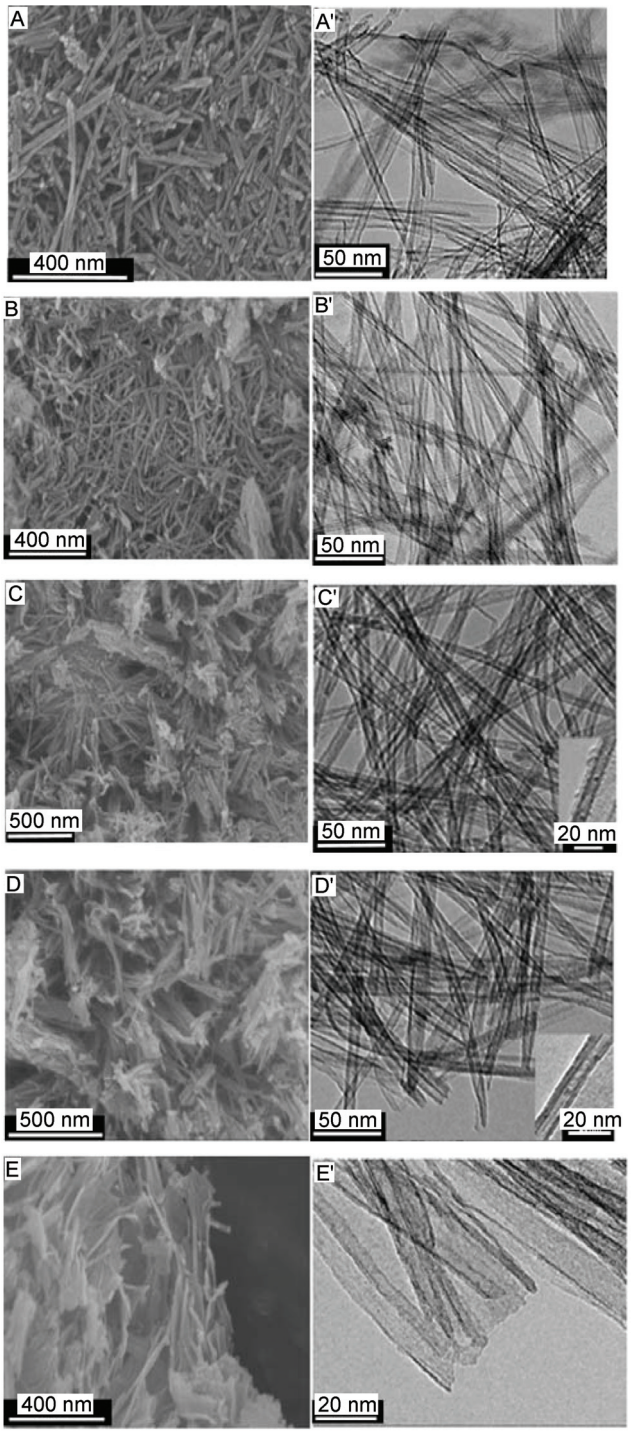

Figure 1 SEM, TEM and HRTEM images of Bi-doped TiO_2 nanaotubes. (A/A') 0.4-BT NTs, (B/B') 0.7-BT NTs, (C/C') 1.0-BT NTs, (D/D') 2.0-BT NTs, (E/E') 5.0-BT NTs.

The XRD patterns of the Bi-doped TiO_2 NTs are shown in Figure 2A. The diffraction peaks of TiO_2 NTs sample are consistent with pure anatase phase (JCPDS: 21-1272). For TiO_2 NTs with lower Bi content (Figure 2A b—e), the crystalline phase is mainly composed of anatase TiO_2. However, the magnified patterns (Figure 2B) show that the (101) peak at 25.0° shifts to a lower degree with the increase of Bi content. This is because the radius of Bi^{3+} ions (0.103 nm) is larger than that of Ti^{4+} ions (0.061 nm). As a result, the distance of nearest-neighbor crystalline plane becomes wider when Bi^{3+} ions replacing Ti^{4+} in TiO_2.[16] Such results demonstrate that Bi cations have been doped into the crystal lattice of TiO_2. In addition, the weak diffraction peaks at 23.9º, 27.8º, 31.7º and 47.7º corresponding to $H_2Ti_2O_5{\bullet}H_2O$ phase (JCPDS: 47-0124) can be observed with the increase of Bi content, and only $H_2Ti_2O_5{\bullet}H_2O$ phase can be found in 5-BT NTs sample, suggesting that the addition of Bi cation hindered the transformation of $H_2Ti_2O_5{\bullet}H_2O$ phase to TiO_2 anatase phase during the acid-washing treatment.

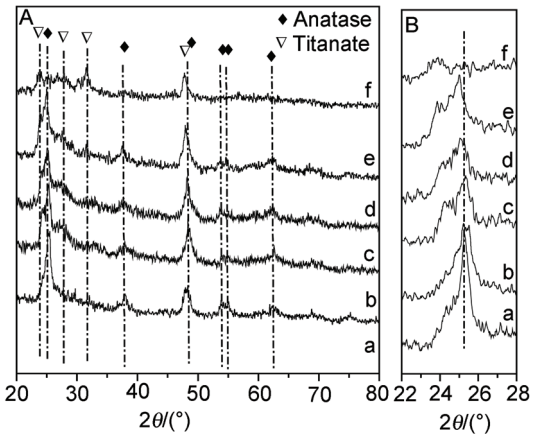

Figure 2 XRD patterns (A), magnified patterns (B) of Bi-TiO_2 nanotubes. (a) TiO_2 NTs; (b) 0.4-BT NTs, (c) 0.7-BT NTs, (d) 1.0-BT NTs; (e) 2.0-BT NTs; (f) 5.0-BT NTs.

Figure 3 shows the Raman spectra of Bi-doped TiO_2 NTs. The Raman peaks at 143.3, 395.3, 513.2 and 639.0 cm^{-1} are attributed to the typical anatase active modes, and the peaks at 272.5, 452.6, 666.4 cm^{-1} are assigned to the titanate nanotubes.[15] This illustrates that the as-prepared TiO_2 NTs are pure anatase phase, and the 5-BT NTs are pure titanate phase. However, other Bi-doped TiO_2 NTs samples contain a mixed phase of titanate and anatase. Besides that, the inset pattern in Figure 3 shows that the Raman peak at 143 cm^{-1} corresponding to Ti-O-Ti frame becomes weak gradually and shifts to a higher position with the increase of Bi content. The shift and weakening of the Raman peaks of Bi-doped titania should be interpreted as the effects of Bi doping, which destroys the symmetry of the Ti-O-Ti network partly by the formation of Ti-O-Bi bond.

To obtain further insight into the surface constitution and the oxidation state of the bismuth dopant in the samples, the Ti 2p and Bi 4f binding energy was investigated. The corresponding spectra are plotted in Figure 4.

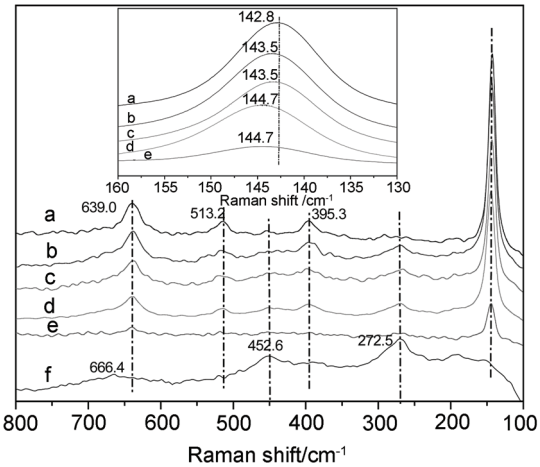

Figure 3 FT-Raman of TO_2 and Bi-TiO_2 nanotubes. (a) TiO_2 NTs; (b) 0.4-BT NTs, (c) 0.7-BT NTs, (d) 1.0-BT NTs; (e) 2.0-BT NTs; (f) 5.0-BT NTs.

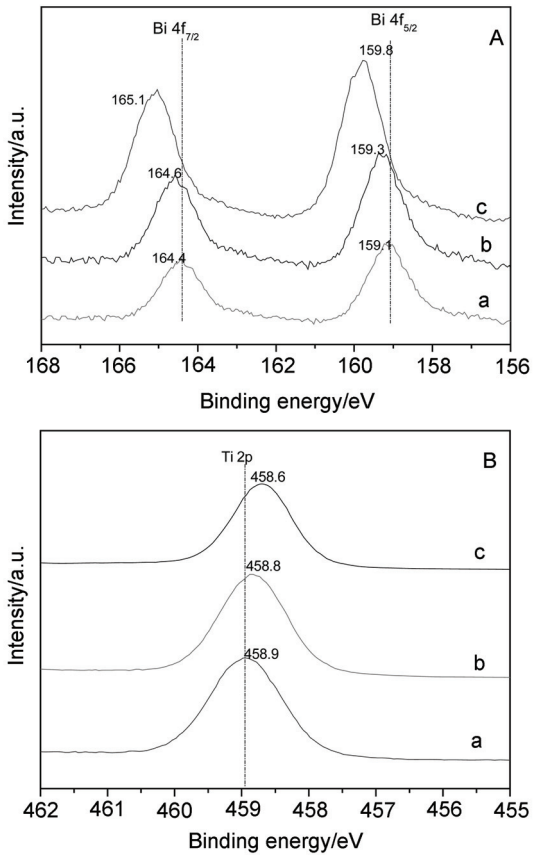

Figure 4 XPS spectra of (A) Bi 4f, (B) Ti 2p. (a) 1.0-BT NTs, (b) 2.0-BT NTs, (c) 5.0-BT NTs.

According to the previous reports, the binding energies of Bi $4f_{7/2}$ and Bi $4f_{5/2}$ for pure Bi_2O_3 at 158.6 and 163.9 eV, respectively, were accepted as standard for the XPS measurement.[15,20] Figure 4A shows that the intensity of the Bi 4f peaks increases and the binding energies of the Bi 4f peaks shift obviously toward higher values with the increase of Bi content. The binding energies of Bi $4f_{7/2}$ and Bi $4f_{5/2}$ for three Bi doped samples are higher than the values of pure Bi_2O_3. The positive shift is attributed to a higher oxidation state of the bismuth dopant ($Bi^{(3+x+)}$ state).[15] It indicates a strong interaction between Bi and TiO_2, and that the Bi^{3+} centers are oxidized to $Bi^{(3+x+)}$. In addition, Figure 4B shows that the binding energy of Ti 2p has a slight decrease with the increase of Bi content. The slight decrease in binding energy of Ti 2p suggests that some Ti^{4+} ions are converted to a lower oxidation state due to the Bi substitutions.[15] The change of oxidation state of Ti and Bi energy may be attributed to the formation of Bi-O-Ti bonds in the framework of titania. These results are consistent with the Raman results.

Figure 5 shows the UV-vis diffuse reflectance absorption spectra of Bi-doped and pure TiO_2 nanotubes. In comparison with that of the undoped TiO_2 NTs, Bi-doped TiO_2 samples have a tail or shoulder absorbance in the visible light region and the tail is more obvious with increasing Bi content, which is consistent with the yellow color of the sample. This result indicates that Bi doping can enlarge the wavelength response range and the effect of Bi doping on visible-light response should be related to the form of Ti-O-Bi in the network of the titania nanotube.

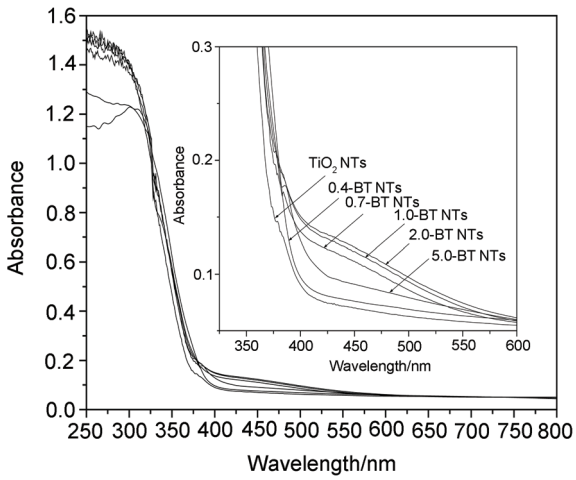

Figure 5 UV-Vis DRS spectra of Bi-TiO_2 nanotubes.

Photocatalytic activities

The photocatalytic performances of the as-prepared samples were evaluated by photocatalytic H_2 evolution rates from glycerol aqueous solution (volume percentage=5%) under the UV light (Hg-Lamp) and solar-simulated light (Xe-Lamp) irradiation. The product analysis showed that only H_2, CO_2, and glycerol were detected, and no any other organic compounds could be found in both gas and liquid products. It is surprising that no oxygen was detected during the splitting of water. However, such phenomena are reasonable in the presence of sacrificial or reducing agents such as glycerol or methanol.[21,22] It is observed that the rates of hydrogen production over all the samples reach a maximum at *ca.* 30 min and then show a steady state even

after 4 h prolonged irradiation. Figure 6 illustrates the steady rates of the photocatalytic H_2 production from glycerol solution in the presence of various samples. It can be seen clearly that the Bi-doped TiO_2 nanotubes exhibit a higher photocatalytic activity than pure TiO_2 nanotubes. The photocatalytic hydrogen evolution rate over the Bi-TiO_2 nanotubes first increases, and then decreases with the increase of Bi content. The 2.0-BT NTs sample exhibits a maximum H_2 production of 4708 $\mu mol \cdot h^{-1} \cdot gcat^{-1}$ under UV light irradiation. Under solar-simulated light irradiation, the 2.0-BT NTs sample is still the most effective catalyst as it results in a maximum of 514 $\mu mol \cdot h^{-1} \cdot gcat^{-1}$. Although the 5.0-BT NTs sample has the highest surface area, the hydrogen evolution rate is lower than that of other Bi-doped TiO_2 nanotubes, revealing that the surface area is not a key factor for photocatalytic hydrogen product. According to the discussion on characterizations mentioned above, the decrease in photocatalytic performance of the 5-BT NTs sample can be attributed to the inferior photocatalytic activity of titanate phase than that of anatase phase and the morphology and structure of the nanobelt.

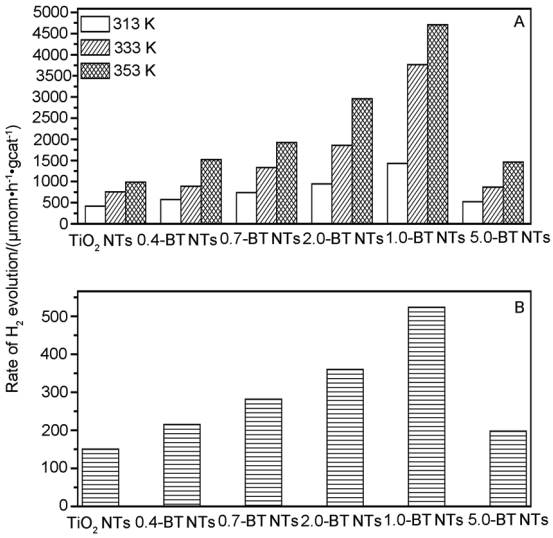

Figure 6 rates of the photocatalytic H_2 evolution from glycerol solution (5%) under UV light (A) at different temperatures and solar-simulated light (B) irradiation at 333 K over Bi-TiO_2 nanotubes.

Compared with pure TiO_2 nanotubes, the superior photocatalytic performance of Bi-doped TiO_2 nanotubes may be ascribed to the Bi-doped ions into TiO_2 nanotubes, which favors the photo absorption and the separation of photo-induced electron-hole pairs. In Bi-doped TiO_2 nanotubes, the bismuth doping creates the $Bi^{(3+x+)}$ species and energy level below the conduction band of TiO_2, which results in a reduction of band-gap energy, as shown in Scheme 1. Under the photo irradiation, BT NTs produces electron-hole pairs at the surface of the photocatalyst; the electrons are trapped by the higher oxidation state Bi dopant ($Bi^{(3+x+)}$), which is converted to Bi^{3+} species, and this aids the separation of the electron-hole pairs. After electron-hole separation, the electrons can be scavenged by H_2O chemisorbed on the surface of catalyst, which in turn is reduced to H_2. The holes can be capture by surface hydroxyl to produce OH radicals, which can further oxidize the glycerol to CO_2 and H_2O. Of course, the holes can also directly oxidize the organic molecules.

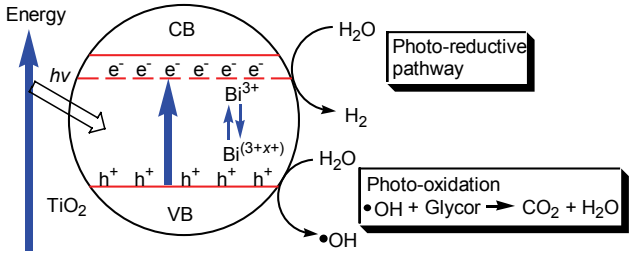

Scheme1 Energy band structure and mechanism of photo-generated carriers transfer of Bi-TiO_2 nanotubes.

Conclusions

The Bi-doped-TiO_2 nanotubes with variable Bi ratios have been successfully synthesized by using hydrothermal treatment in 10 $mol \cdot L^{-1}$ NaOH (aq.) through using Bi-doped TiO_2 particles derived from conventional sol-gel method as starting materials. Bi-doped-TiO_2 samples showed an extension of light absorption into the visible region, which mainly originates from the doping process with the formation of new $Bi^{(3+x+)}$ species and energy level of Bi ion, and reduction of the electron-hole recombination rate. The appropriate Bi-doped content has positive effects on the photocatalytic activity of the TiO_2 nanotubes. Among the as-prepared samples, the 2-BT NTs display the maximum H_2 production under UV and solar-simulated light irradiation. Excessive doping of Bi ions in the crystal structure of TiO_2 results in the transformation of nanotubes with anatase phase to nanobelt composed entirely of titanate phase, which would decrease the catalytic activity for hydrogen production.

Acknowledgement

We acknowledge the financial supports from the National Natural Science Foundation of China (Nos. 21276190 and 20806059).

References

[1] Fujishima, A.; Honda, K. *Nature* **1972**, *238*, 37.
[2] Zou, Z. G.; Ye, J. H.; Sayama, K. *Nature* **2001**, *414*, 625.
[3] Park, J. H.; Kim, S.; Bard, A. J. *Nano Lett.* **2006**, *6*, 24.
[4] Gross, P. A.; Pronkin, S. N.; Cottineau, T. *Catal. Today* **2012**, *189*, 93.
[5] Ganesh, I.; Gupta, A. K.; Kumar, P. P. *Mater. Chem. Phys.* **2012**, *135*, 220.
[6] Guo, G.; Hu, Y.; Jiang, S. *J. Hazard. Mater.* **2012**, *223*, 39.
[7] Wang, X. H.; Zhang, F.; Zheng, Z. H.; Li, C. R. *Mater. Lett.* **2000**, *44*, 105.

[8] Shi, Q.; Yang, D.; Jiang, Z.; Li, J. *J. Mol. Catal. B* **2006**, *43*, 44.
[9] Wang, X. H.; Zhang, F.; Li, C. R.; Zheng, Z. H. *Mater. Lett.* **2000**, *45*, 1.
[10] Hameed, A.; Gombac, V.; Montini, T. *Chem. Phys. Lett.* **2009**, *483*, 254.
[11] Yang, J.; Li, J.; Miao, J. *Chin. J. Inorg. Chem.* **2011**, *27*, 547.
[12] Naik, B.; Parida, K. M.; Behera, G. C. *ChemCatChem* **2011**, *3*, 311.
[13] Xu, J.; Ao, Y.; Fu, D. *Appl. Surf. Sci.* **2008**, *255*, 2365.
[14] Kang, Q.; Yuan, B.; Xu, J.; Fu, M. *Catal. Lett.* **2011**, *141*, 1371.
[15] Sajjad, S.; Sajjad, A. K.; Chen, F.; Zhang, J. L. *Chem. Eur. J.* **2010**, *16*, 13795.
[16] Ji, T. H.; Yang, F.; Lv, Y. Y.; Zhou, J. Y.; Sun, J. Y. *Mater. Lett.* **2009**, *63*, 2044.
[17] Sang, H. X.; Tian, Y.; Wang, X. T.; Tao, L. *J. Inorg. Mater.* **2012**, *12*, 1283.
[18] Sang, H. X.; Wang, X. T.; Fan, C. C.; Wang, F. *Int. J. Hydrogen Energy* **2012**, *37*, 1348.
[19] Hoang, A.; Thuy, L.; Sungmin, C.; Jongsoo, J. *Powder Technol.* **2012**, *225*, 167.
[20] Li, H.; Wang, D.; Wang, P.; Fan, H.; Xie, T. *Chem. Eur. J.* **2009**, *15*, 12521.
[21] Kim, H. G.; Hwang, D. W.; Lee, J. S. *J. Am. Chem. Soc.* **2004**, *126*, 8912.
[22] Daskalaki, V. M.; Kondarides, D. I. *Catal. Today* **2009**, *144*, 75.

(Cheng, F.)

